IOP Publishing Bioinspir. Biomim. 19 (2024) 056010 https://doi.org/10.1088/1748-3190/ad649d

Bioinspiration & Biomimetics

RECEIVED
1 April 2024

REVISED
31 May 2024

ACCEPTED FOR PUBLICATION
17 July 2024

PUBLISHED
29 July 2024

PAPER

Investigation of the tradeoffs between tracking performance and energetics in heterogeneous variable recruitment fluidic artificial muscle bundles

Nicholas Mazzoleni* and Matthew Bryant

Mechanical and Aerospace Engineering, North Carolina State University, Raleigh, NC 27606, United States of America
* Author to whom any correspondence should be addressed.

E-mail: nwmazzol@ncsu.edu

Keywords: fluidic artificial muscles, variable recruitment, Pareto frontier, Henneman's size principle, tradeoff analysis, recruitment order, motor unit size distribution

Abstract

In traditional hydraulic robotics, actuators must be sized for the highest possible load, resulting in significant energy losses when operating in lower force regimes. Variable recruitment fluidic artificial muscle (FAM) bundles offer a novel bio-inspired solution to this problem. Divided into individual MUs, each with its own control valve, a variable recruitment FAM bundle uses a switching control scheme to selectively bring MUs online according to load demand. To date, every dynamic variable recruitment study in the literature has considered homogeneous bundles containing MUs of equal size. However, natural mammalian muscle MUs are heterogeneous and primarily operate based on Henneman's size principle, which states that MUs are recruited from smallest to largest for a given task. Is it better for a FAM variable recruitment bundle to operate according to this principle, or are there other recruitment orders that result in better performance? What are the appropriate criteria for switching between recruitment states for these different recruitment orders? This paper seeks to answer these questions by performing two case studies exploring different bundle MU size distributions, analyzing the tradeoffs between tracking performance and energetics, and determining how these tradeoffs are affected by different MU recruitment order and recruitment state transition thresholds. The only difference between the two test cases is the overall force capacity (i.e. total size) of the bundle. For each test case, a Pareto frontier for different MU size distributions, recruitment orders, and recruitment state transition thresholds is constructed. The results show that there is a complex relationship between overall bundle size, MU size distributions, recruitment orders, and recruitment state transition thresholds corresponding to the best tradeoffs change along the Pareto frontier. Overall, these two case studies validate the use of Henneman's Size Principle as a variable recruitment strategy, but also demonstrate that it should not be the only variable recruitment method considered. They also motivate the need for a more complex variable recruitment scheme that dynamically changes the recruitment state transition threshold and recruitment order based on loading conditions and known system states, along with a co-design problem that optimizes total bundle size and MU size distribution.

1. Introduction

1.1. An overview of mammalian muscle-inspired recruitment in mobile robotics

Considering the wide range of motions that can be achieved seemingly effortlessly by human skeletal muscles, it is no surprise that one of the primary goals of mobile robotics over the past few decades has been to mimic the behavior of these muscles as closely as possible. One of the ways through which this has been achieved has been through the imitation of the hierarchical structure of mammalian muscle.

This structure is inherently redundant, as each muscle consists of thousands of MUs (groups of muscles fibers, sometimes as few as three) with their own nerve ending that can be activated independently of one another [1]. Muscle force can be increased either by increasing the neurological excitation rate of a particular MU, or through the *recruitment* of new MUs [1].

In the literature, the concept of muscle-inspired actuator recruitment is leveraged to achieve several different goals. For example, Mathijssen *et al* develop a compliant solenoid-based actuator that uses recruitment to achieve variable stiffness and redundancy in the case of failure [2]. Odhner and Asada also frame the concept of recruitment as a way to achieve a desired force behavior through a redundant actuation scheme using an SMA-based artificial muscle [3]. Corrado de Pascali *et al* employ the concept of recruitment on pneumatic 3D printed actuators in parallel, bipennate, and fusiform topologies to illustrate that using recruitment allows for regulation of force without changing actuator contraction. The most common application of muscle-inspired recruitment is in hydraulic mobile robotics. In conventional hydraulic actuation systems, the actuator must be sized based on the maximum force required by its application. When lower forces are needed, the actuator pressure must be throttled by a valve to a lower pressure, which results in significant energy losses. Therefore, the closer that an actuator can operate to its source pressure, the more efficient it will be. Bai *et al* apply muscle-inspired recruitment to a conventional hydraulic piston-cylinder system by creating a piston with multiple chambers, each of which can be independently pressurized to better match changing force demands [4]. However, the most prevalent implementation of muscle-inspired recruitment is in fluidic artificial muscles (FAMs), otherwise known as McKibben muscles. A typical FAM consists of an elastic bladder surrounded by a braided mesh which, when pressurized, expands radially and contracts axially, generating a tensile force. Although the mechanism through which FAMs are actuated is different from that of biological muscles, the similarity of their force-length characteristics to those of biological muscles makes them a good choice for biologically inspired actuation systems. In FAM literature, the hierarchical muscle-inspired recruitment of actuators is more specifically referred to as *variable recruitment*, so this term will be adopted for the remainder of this paper.

A variable recruitment bundle consists of a *single* '*actuator tissue*' with multiple FAMs that can be selectively pressurized ('recruited') or depressurized ('derecruited') by the control system to actuate a *single joint*. The FAMs within the bundle can be sequentially based on required load, allowing them to operate much closer to source pressure, increasing overall efficiency. This was first shown to be true for a bundle in quasistatic conditions [5], and was later shown in both dynamic simulation and experimental studies [6–10]. Variable recruitment studies have been performed for both pneumatic and hydraulic artificial muscles bundles, both of which offer certain advantages. Pneumatic artificial muscles are cleaner, do not require a hydraulic reservoir, and offer the potential for reduced weight in a mobile robotics application. However, from an efficiency standpoint, it is more desirable to consider the hydraulic case, as the incompressibility of hydraulic fluid inherently leads to greater efficiency [11]. Therefore, most variable recruitment studies that focus heavily on energy consumption or efficiency consider hydraulically actuated FAMs. In fact, several system-level analyses have been performed (in which hydraulic system components such as the pump, accumulator, and servovalves are considered) to study how the benefits of variable recruitment are affected by electrohydraulic coupling, and have found that variable recruitment can increase overall hydraulic system efficiency and bandwidth [12, 13].

1.2. Gaps in the current literature and motivation for study

Previous dynamic variable recruitment studies, whether in experiments or in simulations, have limited their scopes to bundles containing MUs of the same size, while in mammalian skeletal muscle, MUs vary in size. As a general rule, these MUs are recruited according to Henneman's size principle, which states that MUs are recruited in the order of smallest to largest [14]. However, recent musculoskeletal studies have shown that there may be exceptions to Henneman's size principle in which MUs are recruited in a different order [15–17]. Since no studies have been performed for heterogeneous FAM bundles, the question of whether a Henneman-based approach is desirable for FAM variable recruitment bundles remains unanswered. Another relatively unexplored aspect of variable recruitment is the criterion used to shift between MU activation levels (also known as *recruitment states*). Some studies wait to transition until a MU has completely saturated [6], while others use certain activation thresholds (determined ad hoc) to decide when the next MU should be recruited [7]. A more thorough exploration of how recruitment state transition points should be determined is needed to more optimally design variable recruitment controllers.

To address these gaps in the literature, dynamic system-level electrohydraulic simulations are performed for heterogeneous variable recruitment bundles. In these simulations, three important parameters are varied for a bundle while keeping its

maximum force output and electrohydraulic system parameters constant:

1. The fraction of the total bundle force that each MU can contribute, called the *MU size distribution*.
2. The order in which each MU is recruited (e.g. Smallest→Medium→Largest, Largest → Medium → etc)
3. The pressure at which a new MU is recruited, also known as the *recruitment state transition threshold*.

The purpose of these simulations is to develop an understanding of how the variation of these three different factors affects the overall tracking and energetic performance of the system. For each different MU size distribution, a Pareto frontier is developed that shows the performance-energetics tradeoffs associated with the recruitment orders and recruitment state transition thresholds for that distribution. These tradeoffs are then compared across different MU force distributions to determine a global Pareto frontier, which can be viewed as a co-design tool with the goal of determining the optimal individual MU sizing within a given bundle. This study is performed for two case studies with different total bundle force capacities, and the results are compared.

The remainder of this paper is laid out as follows. Section 2 defines the robotic system of interest and the generalized recruitment architecture for this study. Section 3 outlines a model of the electrohydraulic system used in the study. Section 4 provides more details regarding the study methodology, shows results for both test cases, and discusses the implications of those results. Finally, section 5 offers final conclusions and suggestions for how the study can be expanded in future work.

2. Variable recruitment control architecture

2.1. Defining a robotic system of interest

Consider a heterogeneous variable recruitment bundle consisting of three motor units (MUs) actuating a simple 1-DOF robotic arm. The bundle and the arm are shown in figure 1.

A well-documented phenomenon associated exclusively with variable recruitment is the buckling of inactive MUs during contraction in lower recruitment states. This phenomenon is undesirable because it results in the generation of resistive forces that reduce overall bundle force output and reduces total bundle volumetric energy density [18, 19]. In this study, it is assumed that each MU is attached to a flexible but inextensible tendon that prevents it from ever going into compression when inactive or at a low pressure. This mitigation technique allows resistive forces to be neglected, simplifying the system modeling [19].

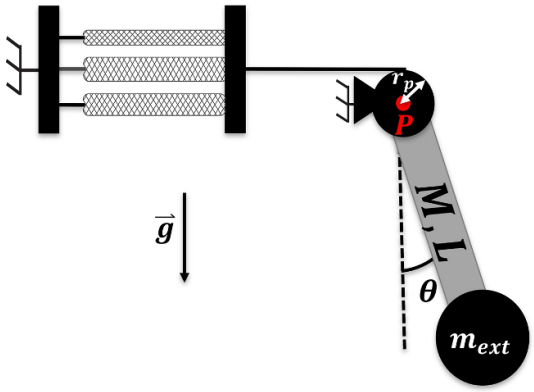

Figure 1. 1-DOF arm actuated by heterogeneous 3-MU variable recruitment bundle. The arm has a mass M and length L. There is an external mass m_{ext} attached to the arm that represents a specific payload or task for the robotic arm to complete. The arm is attached to a pulley of radius r_{p}, and the FAM bundle is attached to this pulley and exerts a torque on the arm through the pulley.

The 1-DOF arm can be modeled like a compound pendulum, using the following equation of motion:

$$J\ddot{\theta} = F_{\text{FAM}} r_{\text{p}} - b\dot{\theta} - Mg\frac{L}{2}\sin\theta - m_{\text{ext}} gL\sin\theta \quad (1)$$

where J is the mass moment of inertia, F_{FAM} is the total force exerted on the arm by the FAM bundle, r_{p} is the arm pulley radius, b is the damping coefficient, M is the total mass of the arm, m_{ext} is the external (load) mass at the end of the arm, g is the acceleration due to gravity, and L is the total length of the arm.

Each MU in the bundle exerts a force according to a corrected version of the Tondu ideal FAM model [20] that uses the experimentally determined blocked force and free strain of a FAM with the same radius, length and initial braid angle as the one in the model to improve accuracy. This model is given by the following equation:

$$F = k_{\text{F}} \pi r_0^2 P_{\text{MU}} \left(a(1 - k_\varepsilon \varepsilon)^2 - b \right) \quad (2)$$

where k_{F} is the blocked force empirical correction factor, k_ε is the free strain empirical correction factor, P_{MU} is the MU pressure, r_0 is the initial outer radius of the FAM, L_0 is the initial length of the FAM, ε is the FAM strain (the ratio of muscle contraction to initial FAM length), and a and b are braid angle-dependent kinematic parameters:

$$a = \frac{3}{\tan^2\alpha_0} \quad (3)$$

$$b = \frac{1}{\sin^2\alpha_0}. \quad (4)$$

Although many different curve-fit equations can be used for the correction factor terms, in this paper, the ones used are from Meller *et al* [7], and are given by:

$$k_{\text{F}} = \text{constant} \quad (5)$$

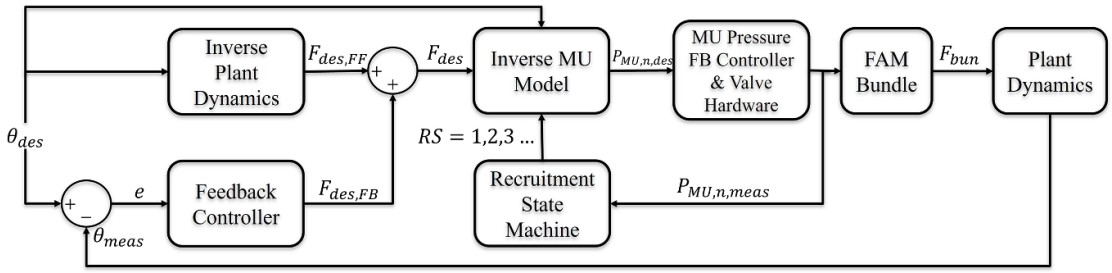

Figure 2. High-level variable recruitment controller. The controller uses model-based feedforward control but also has outer loop and inner loop P controllers to account for lag and system dynamics. An inverse model of the 1-DOF robotic limb is used to generate a feedforward force command for the bundle. Inverse models of the FAMs in the bundle are used to generate desired pressures for each MU based on the desired force, desired strain (which is a function of the desired trajectory angle) and recruitment state. Each desired pressure goes to a P-controller (with a gain of 0.0005 V/Pa) that controls the pressure in each MU by adjusting the spool position of an electrohydraulic servovalve. The measured pressures in each MU are used to determine the recruitment state through state machine logic. The measured angle of the 1-DOF robotic limb is fed back to a P controller (with a gain of 50 N rad^{-1}), which adjusts the desired force according to the tracking error.

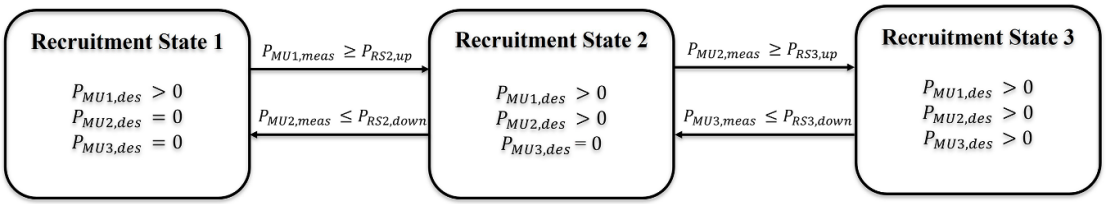

Figure 3. Generalized variable recruitment scheme for a 3-MU bundle. When the pressure in MU1, $P_{MU1,meas}$, exceeds the upshift recruitment state transition threshold, $P_{RS2,up}$, MU2 is recruited and the bundle enters RS2. The same logic applies for the transition from RS2 to RS3. Transitions can also occur from a higher recruitment state to a lower recruitment state. For example, if $P_{MU3,meas}$ falls below $P_{RS3,down}$, then the bundle transitions from RS3 to RS2.

$$k_\varepsilon = 1 + a_{k\varepsilon} e^{-b_{k\varepsilon} P} \tag{6}$$

where $a_{k\varepsilon}$ and $b_{k\varepsilon}$ are both constants. The advantage of this model, commonly used in variable recruitment literature [6, 7], is that it does not require any physics-based understanding of FAM properties (such as bladder elasticity) or knowledge of parameters that would be difficult to determine accurately. However, the disadvantage of it is that because it requires an experimental characterization of the blocked force and free strain characteristics of a particular FAM, it is only valid for a FAM with those parameters. For this study, this is not an issue, because it will be assumed that although each MU is a different size, the FAMs within each individual MU are identical, requiring only one set of experiments to determine the empirical correction factors.

2.2. Generalized variable recruitment architecture

The control scheme for the robotic arm's motion, shown in figure 2, consists of a feedforward term and two feedback loops. The feedforward term is calculated using the desired plant angular position, the inverse arm dynamics, and the arm pulley radius to calculate the force required to achieve the desired arm motion. It contains an inner feedback loop that controls the pressure in each MU and an outer force feedback loop that accounts for errors in angular position due to pressure dynamics or model mismatches.

The desired pressure for each MU is calculated using an inverse model of the MUs in the variable recruitment bundle. This model receives the desired force, which is the sum of the feedback force and the feedforward force terms, the desired strain (which is directly proportional to the desired arm angle) and the current recruitment state of the bundle, and outputs the desired pressure to each MU. The recruitment scheme is executed using a finite state machine, the logic for which is shown in figure 3.

In recruitment state 1 (RS1), MU1 is the only active MU. The bundle remains in RS1 until the pressure in MU1 exceeds a certain threshold percent of the maximum source pressure (called the *recruitment state transition threshold*), at which point the bundle enters RS2 and MU2 is activated. Similarly, when the pressure in MU2 exceeds the recruitment state transition threshold for RS3, the bundle enters RS3 and MU3 is activated. The bundle can also downshift from a higher recruitment state to a lower recruitment state if the pressure in that MU decreases below a given threshold.

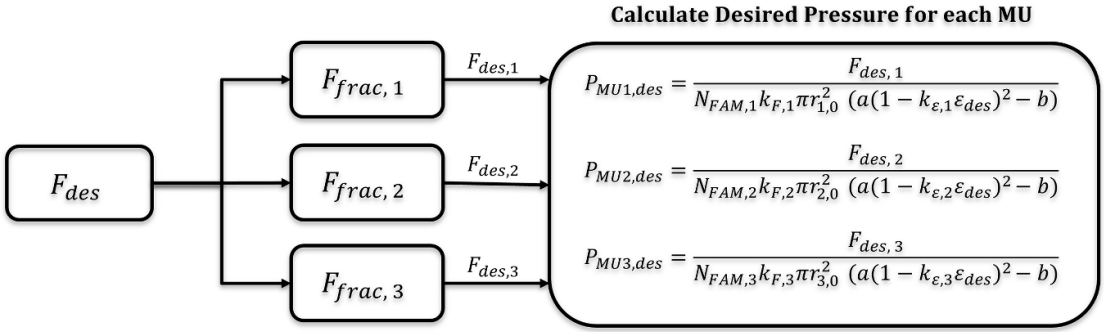

Figure 4. Generalized force allocation scheme for a heterogeneous variable recruitment bundle. Each MU has an initial radius denoted by $r_{n,0}$, where n represents the nth MU. A fraction of the overall desired force F_{des} is allocated to each MU through $F_{\text{frac},n}$. The desired pressure in each MU is then determined based on the desired force to that MU and the desired strain using an inverse model of the FAM.

For an idealized variable recruitment bundle, there would be no need for a recruitment transition threshold. Instead, recruitment transitions would simply be triggered once the MU pressure reached 100% of the source pressure and the system would track the desired trajectory perfectly. However, in an actual system, one must consider valve spool dynamics, the nonlinearity of the valve flow rate, MU pressure dynamics, the deslacking of newly recruited MUs, and feedforward model mismatches, all of which introduce significant error to the system. To address this, recruitment upshift thresholds $P_{\text{RS2,up}}$ and $P_{\text{RS3,up}}$ are introduced. These thresholds determine when the bundle should shift between recruitment states and can be set anywhere between 0% of the source pressure (all MUs active from the very beginning and no variable recruitment) or 100% of the source pressure (recruitment transition does not occur until MU pressure saturates for a given recruitment state). These thresholds are implemented in Meller *et al* and are chosen *ad hoc* based on system performance [7]. In Vemula *et al*, recruitment thresholds are used, but only to eliminate slack from MUs before they are recruited, not to provide additional force capabilities before a previously recruited MU reaches saturation [10].

The desired force in each MU for a given recruitment state can be allocated in many ways, especially for a bundle with differently sized MUs. The generalized form of the desired MU force allocation scheme is shown in figure 4.

In this scheme, a certain fraction $F_{\text{frac},n}$ of the desired force is allocated to each active MU (if an MU is not yet active, this fraction is equal to zero by default). This force allocation can be different for each MU and it can change over time. The simplest way to allocate force to each active MU is to make the force distribution fraction of each active MU directly proportional to the ratio of the individual MU area to the overall active area of the bundle, as shown in the following equations:

$$F_{\text{frac},1} = \frac{A_{\text{MU1}}}{A_{\text{bun, act}}} \tag{7}$$

$$F_{\text{frac},2} = \frac{A_{\text{MU2}}}{A_{\text{bun, act}}},\ \text{RS} > 1 \tag{8}$$

$$F_{\text{frac},3} = \frac{A_{\text{MU3}}}{A_{\text{bun, act}}},\ \text{RS} > 2 \tag{9}$$

where $A_{\text{bun, act}}$ is total area of active MUs within the bundle, which is a function of the current recruitment state. Because the FAM force is linearly dependent on cross-sectional area and upon pressure, when this MU force allocation scheme is used, the desired pressures in each active MU for a given recruitment state are equivalent. This is similar to the 'batch' recruitment scheme that has been proposed in other studies [6, 7]. If another MU force allocation scheme was used, the desired pressure in all three MUs would be different. For this study, the batch recruitment scheme is implemented due to its simplicity and its similarity to other schemes already implemented in the literature.

The calculate the desired pressure in a MU for a specified motion trajectory, equation (2) can be inverted to give the following equation:

$$P_{\text{MU},n,\text{des}} = \frac{(F_{\text{des}})\,(F_{\text{frac},n})}{N_{\text{FAM},n}k_{\text{F},n}\pi\, r_{n,0}^2\left(a(1-k_{\varepsilon,n}\varepsilon_{\text{des}})^2 - b\right)} \tag{10}$$

where F_{des} is the total desired force required from the bundle and N_{FAM}, n is the is the number of FAMs in the nth MU. From the equation, it can be observed that $P_{\text{MU},n,\text{des}}$ is a function of both desired bundle force and desired bundle strain, requiring the use of either an iterative solver or lookup table.

3. Electrohydraulic system modeling

In a realistic, non-idealized electrohydraulic robotic system, the hydraulic pump (and the electric motor

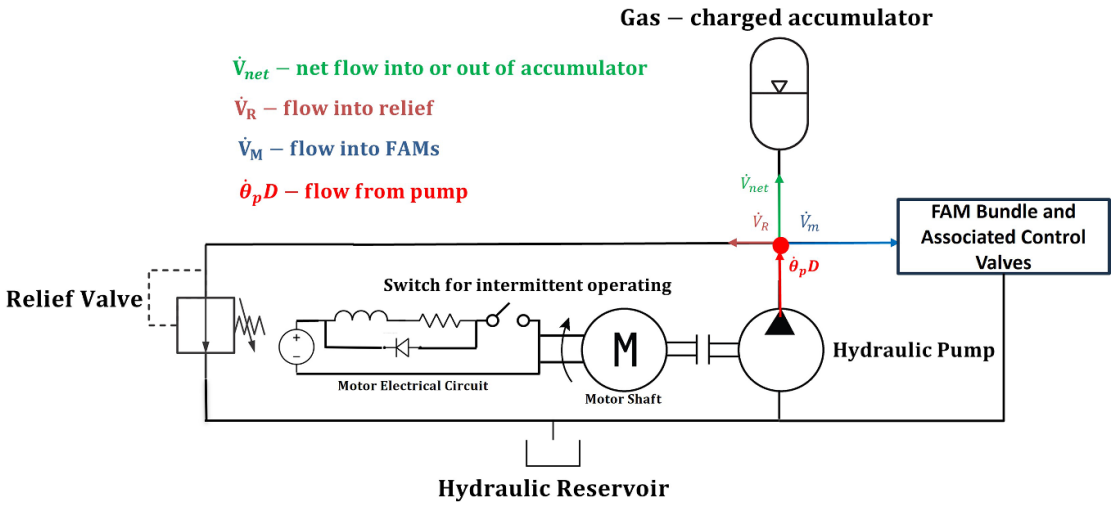

Figure 5. Hydraulic circuit diagram. The hydraulic circuit consists of a hydraulic pump driven by an electric motor circuit that can be switched on and off to allow for intermittent operation, a gas-charged accumulator, a relief valve, the FAM MUs and their corresponding control valves.

used to drive it), accumulator, and valve dynamics play a significant role in determining system performance, and it is necessary to build a system-level model with sufficient fidelity to capture these effects. The electrohydraulic system model developed by Chapman *et al* and Kim *et al* to analyze system-level performance is adapted for this study, with a few important modifications from their original work [12, 13].

3.1. Electrohydraulic system—motor-pump and accumulator equations

A diagram of the electrohydraulic circuit is shown in figure 5.

The circuit is driven by a motor-pump assembly connected to a gas-charged accumulator. The purpose of the accumulator is to store hydraulic fluid at a given pressure and release it when it is needed by the system. The output of the accumulator is connected to each FAM MU in a variable recruitment bundle. The motor-pump assembly is also connected to a relief valve. The purpose of this relief valve is to ensure that the accumulator pressure remains at or below its maximum pressure regardless of the flow rate supplied by the pump or demanded by the FAM bundle. The pressure of each MU is controlled by a two-stage servo-valve.

The motor-pump assembly is governed by the standard electromechanical equations for a DC motor. The electrical equation is given by the following:

$$\frac{\mathrm{d}I}{\mathrm{d}t} = \frac{1}{L}\left(V - IR - k_\mathrm{b}\dot{\theta}\right) \tag{11}$$

where V is the constant voltage supplied to the motor, I is the current supplied to the motor, L is the motor inductance, R is the motor resistance, k_b is the motor back EMF constant, and $\dot{\theta}$ is the rotational speed of the motor. The mechanical equation is given by:

$$\ddot{\theta}_\mathrm{p} = \frac{1}{J_\mathrm{p}}\left(k_\mathrm{e} I - B_\mathrm{p}\dot{\theta}_\mathrm{p} - \tau_\mathrm{p}\right) \tag{12}$$

where J is the mass moment of inertia of the motor shaft, k_e is the motor torque constant, B_p is the motor damping constant, and τ_p is the torque that acts on the motor shaft due to the pump impeller. This torque is given by:

$$\tau_\mathrm{p} = P_\mathrm{acc} D \tag{13}$$

where P_acc is the accumulator pressure and D is the pump displacement. It is important to note that in this equation, the units for pump displacement are in $\mathrm{m}^3\ \mathrm{rad}^{-1}$, while many times pump displacement is expressed in mL/rev. Pump displacement is used to calculate the flow rate:

$$Q = \dot{\theta}_\mathrm{p} D. \tag{14}$$

Because of the impeller torque term in the mechanical equation, the performance of the motor-pump assembly (flow rate, current draw, etc) is coupled with the pressure in the accumulator. This pressure is a function of both the volume input to the accumulator from the pump and the volume drawn from the pump by the FAM MUs. The equation for pressure can be derived using the constant-temperature ideal gas law relation that relates change in pressure to change in volume:

$$P_\mathrm{acc} = \frac{P_\mathrm{acc,max} V_\mathrm{acc,max}}{V_\mathrm{acc,max} - V_\mathrm{net}} \tag{15}$$

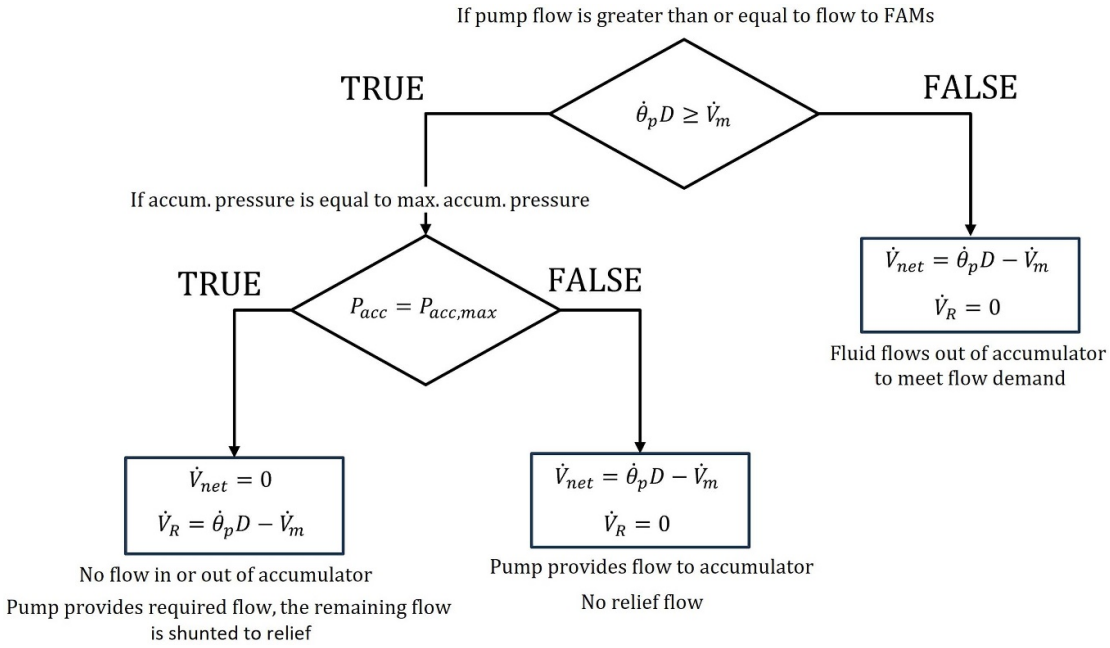

Figure 6. Hydraulic relief valve logic. This logic determines the net flow rate into the accumulator and relief based on the instantaneous flow demand from the FAMs and the instantaneous pressure in the accumulator.

where $P_{\text{acc,max}}$ and $V_{\text{acc,max}}$ are the maximum pressure and volume of the gas in the accumulator, respectively, and V_{net} is the net volume of fluid added or drawn from the accumulator. To keep the accumulator pressure at or below its maximum pressure, a relief valve must be used. The relief valve can be modeled quasistatically using simple if-logic for the flow rate of the motor-pump assembly, shown in figure 6.

This logic ensures that if the pressure is at or exceeds the maximum accumulator pressure, the flow rate is constrained such that the pressure remains or quickly returns to that maximum value. Any remaining flow passes through the relief valve to the reservoir.

Previous studies have shown that the system-level efficiency benefits of variable recruitment are most pronounced when the motor-pump-accumulator assembly is operated intermittently during cyclic motion of the robotic system of interest [12, 13]. For intermittent pump operation, electrical power is only supplied to the pump once the accumulator has been sufficiently depleted. Once this occurs and the pump turns on, it runs until the accumulator pressure is restored to its maximum value, at which time it turns off. This operation mode saves energy by only operating the pump only when necessary.

The condition for turning on the pump is when the accumulator pressure is less than or equal to 99% of the maximum accumulator pressure. This threshold is chosen to prevent chattering when the pump initially turns on. When the accumulator pressure recovers to its maximum value, the pump turns off, and the current supplied to the pump becomes zero. However, because the voltage and motor shaft velocity are nonzero, the derivative of current is nonzero. This effect is undesirable, so it is assumed that the electrical circuit for the motor-pump has a flyback diode that prevents this from happening. The practical effect of this assumption in the dynamic model of the motor-pump assembly is that it sets the derivative of motor current equal to zero when the pump is turned off.

3.2. Electrohydraulic system: valve flow and pressure dynamics

The pressure of each individual FAM bundle MU is controlled by a two-stage pilot-driven electrohydraulic servovalve. The equation for flow rate from the accumulator through the valve is given by the following if/else logic statement:

$$Q_{\text{v}} = c_{\text{v}} x_{\text{v}} \text{sign}\left(P_{\text{acc}} - P_{\text{v}}\right) \sqrt{|P_{\text{acc}} - P_{\text{v}}|}, \quad \textit{if } x_{\text{v}} > 0$$

$$Q_{\text{v}} = c_{\text{v}} x_{\text{v}} \text{sign}\left(P_{\text{v}} - P_{\text{T}}\right) \sqrt{|P_{\text{v}} - P_{\text{T}}|}, \quad \textit{if } x_{\text{v}} < 0$$

$$Q_{\text{v}} = 0, \quad \text{otherwise} \tag{16}$$

where c_{v} is the valve coefficient, x_{v} is the valve spool displacement, P_{v} is the pressure immediately downstream of the servovalve, and P_{T} is the pressure of the fluid reservoir (for an ideal reservoir this pressure is equal to zero). The motion of the servovalve spool can be represented using a second-order dynamic model, but in this paper, it is assumed that the dynamics of the spool are negligible, making the spool position directly proportional to the input voltage given to

the valve. The valve coefficient can be approximated using the nominal flow information from the valve's datasheet:

$$c_v = \frac{Q_N}{\sqrt{\Delta P_N/2}x_{v,max}} \tag{17}$$

where Q_N is the nominal flow rate across the valve, $\sqrt{\Delta P_N}$ is the nominal pressure drop across the valve, and $x_{v,max}$ is the maximum valve position.

The pressure directly downstream of the valve is governed by the following differential equation:

$$\frac{dP_v}{dt} = E'\frac{Q_v - \dot{V}_v}{V_v} \tag{18}$$

where E' is the effective bulk modulus of the hydraulic fluid, V_v is the volume of fluid in the conduit between the valve and its associated FAM MU. In this paper, this volume is assumed to be constant, which implies that $\dot{V}_v$ is equal to zero. If the conduit radius and length are known, then the volume of the conduit can readily be calculated.

As a result of the conduit, the instantaneous pressure immediately downstream of the servovalve and the instantaneous pressure in an individual MU are not the same. The flow rate into an individual MU as a result of this pressure difference is given by the Hagen–Poiseuille equation for steady and laminar flow [21]:

$$Q_{MU} = \frac{\pi r_{c,down}^4 (P_v - P_{MU})}{8\eta L_{c,down}} \tag{19}$$

where $r_{c,down}$ is the downstream conduit radius, $L_{c,down}$ is the downstream conduit length, η is the dynamic viscosity of hydraulic oil, and P_{MU} is MU pressure. In a system with variable recruitment, the equation governing the pressure growth inside of an individual MU is more complex than the one governing pressure growth downstream of the servovalve due to the nature of variable recruitment and the pressure-dependent free strain observed in non-idealized FAMs. These pressure dynamics will be discussed in full detail in the next section.

3.3. MU pressure dynamics and the de-slacking of newly recruited MUs

The pressure dynamics of MU1 (i.e. the first MU recruited in a variable recruitment bundle), are given by an equation that is very similar to the one for the pressure growth directly downstream of the servovalve:

$$\frac{dP_{MU}}{dt} = E'\frac{Q_{MU} - \dot{V}_{MU}}{V_{MU}} \tag{20}$$

where V_{MU} is the volume inside of the MU. An expression for this volume, developed by Tondu and Lopez [22], is given by the following:

$$V_{MU} = \pi r_0^2 L_0 \left[b(1-\varepsilon) - a\left(3(1-\varepsilon)^3\right)\right]. \tag{21}$$

The equation for the rate of change of this volume is thus given by:

$$\dot{V}_{MU} = \pi r_0^2 \dot{x}_m \left[a\left(1 - \frac{x_m}{L_0}\right)^2 - b)\right] \tag{22}$$

where x_m is equal to the MU contraction.

The pressure dynamics for subsequently recruited MUs are more complicated than they are for the first MU. When a new MU is recruited, its contraction is initially zero, while the bundle contraction may be greater than zero. Due to the pressure-dependent free contraction behavior of the MU, it will not begin to generate force until its internal pressure becomes sufficiently large for its contraction to equal that of the bundle. This is known as 'de-slacking' [10, 19]. During de-slacking, it is assumed that the force on the MU is zero, and thus the pressure in the MU is equal to the free contraction pressure corresponding to the MU's instantaneous length. Once the contraction of the MU catches up to that of the overall bundle, the pressure dynamics of that MU follow equation (20).

4. Simulation case studies: exploring effect of MU size distribution, recruitment state transition threshold, and recruiment order

4.1. Methodology

A dynamic simulation study is designed to characterize the tradeoffs between tracking performance and energetics for a variety of different MU sizes, MU recruitment orders, and recruitment state transition thresholds for a given set of dynamic system, trajectory, and electrohydraulic system parameters.

The system-of-interest (shown in figure 1) is commanded to track a sine wave trajectory from 0 to 30 degrees at a specified frequency. This trajectory is based on a standard trajectory for FAM-based robotics in previous variable recruitment simulation studies [12, 13]. For a given test case, the total maximum bundle cross-sectional area is kept constant and is chosen based on the desired ratio of the bundle blocked force to the maximum force required to perform the desired trajectory for the specified dynamic system. However, the way in which this area is distributed within the bundle is varied. In a particular test case, each MU is assigned a certain fraction of the overall bundle area, which determines its size. The MU size distributions used for this simulation study are shown in table 1. It is worth noting that the results for each size distribution will be compared to a baseline case, in which each MU is the same size.

The MU size distributions are chosen specifically to provide a range of size differences between the largest MU and the size of the smallest MU. As

Table 1. MU size distributions (as a fraction of overall bundle force) for simulation study.

	Smallest MU	Medium MU	Largest MU
MU size distribution 1	0.1	0.15	0.75
MU size distribution 2	0.1	0.3	0.6
MU size distribution 3	0.25	0.3	0.45

mentioned previously, to achieve different recruitment behavior, the percentage of the desired force, or *MU force distribution*, can be allocated differently to different MUs to achieve different recruitment behavior. For this study, the MU force distribution used is the same as the MU size distribution, resulting in the 'batch' recruitment scheme, where the desired pressures in each active MU are equivalent. In addition to sweeping through different MU size distributions, this study also examines the effects of different *recruitment orders*. For a bundle consisting of three MUs, there are six possible recruitment orders (note that for equally sized MUs, these six recruitment orders will yield identical results).

Finally, for each combination of MU size distribution and recruitment order, the recruitment state transition thresholds for RS2 and RS3 are varied independently from 0%–90% of maximum accumulator pressure, resulting in 100 different recruitment state transition threshold combinations. The results of each test case are evaluated using a tracking performance metric and a system energetics metric. The tracking performance metric is based on the integrated absolute error (IAE) between the actual arm angle θ_{act} and the desired arm angle θ_{des}:

$$\text{IAE} = \int_0^{t_f} (|\theta_{\text{act}} - \theta_{\text{des}}|)\, \mathrm{d}t. \tag{23}$$

The energetics performance metric is based on the amount of electrical energy consumed by the motor-pump assembly in a single motion cycle, given by:

$$E_{\text{motor}} = \int_0^{t_f} (VI)\, \mathrm{d}t. \tag{24}$$

For each test case, these performance metrics are plotted against one another, and the Pareto frontier is determined, displaying the tradeoffs between the two metrics for a given set of MU size distributions and/or recruitment orders.

The parameters used for the simulation study can be summarized in the following set of tables.

Table 2. Fixed FAM parameters used for both case studies.

L_0 (m)	α_0 (rad)	$N_{\text{FAM},n}$	$a_{k\varepsilon,n}$	$k_{\text{F},n}$	$b_{k\varepsilon,n}$
0.2286 (9 in)	0.5760	1	200	0.7	0.2

Table 2 shows the FAM parameters used for the study. The FAM length and braid angle parameters are chosen to be reasonable for a typical mobile robotics application, and the correction factor parameters are chosen to be representative of the force-strain behavior commonly observed in FAMs with elastic bladder material [5, 7]. The correction factors for each FAM in the bundle are assumed to be the same. For the first case study, the total bundle cross-sectional area (i.e. the sum of the cross-sectional area of each individual MU) is kept fixed at 466 mm^2, and the MUs in for each size distribution are sized based on this total area. This area is chosen such that ratio of the maximum bundle blocked force to the maximum required trajectory force is approximately equal to 2. For the second case study, the bundle total cross-sectional area is doubled, making this ratio equal to 4.

Table 3. Fixed SDOF robotic arm parameters used for each test case.

M (kg)	L (m)	ζ	m_{ext} (kg)	r_{p} (m)
12.5	0.452	0.01	5	0.05

Table 3 contains the robotic arm parameters used for the study. The robotic arm mass and length parameters are approximately representative of the leg mass and length of a human male who weighs 75 kg and is 183 cm tall [23]. The external load mass is chosen not based on any physical quantity but is simply chosen to provide additional torque to resist motion.

Table 4. Fixed motor parameters used for each test case.

V_{motor} (V)	R (Ω)	L (mH)	k_{e} (N·m A^{-1})	k_{b} (V·s rad^{-1})	J_{p} (kg·m^2)	B_{p} (N·m·s rad^{-1})
12	1.250	89	0.0171	0.028	4.2×10^{-7}	1.74×10^{-7}

Tables 4 and 5 contain the electrohydraulic system parameters, which are chosen to be similar to those used in previous system-level electrohydraulic studies [12, 13].

Table 5. Fixed pump/valve/accumulator hydraulic parameters used for each test case.

$P_{acc,max}$ (kPa)	$V_{acc,max}$ (m^3)	E_{max} (kPa)	η ($N{\cdot}s\ m^{-2}$)	D ($m^3\ rad^{-2}$)
689.48 (100 psi)	0.0001	1800	0.2742	5.0930×10^{-8}
ΔP_N (kPa)	$x_{v,max}$ (m)	Q_N ($m^3\ s^{-1}$)	$r_{c,down}$ (m)	$L_{c,down}$ (m)
3500	0.007 92	0.000 95	0.006 25	0.4572

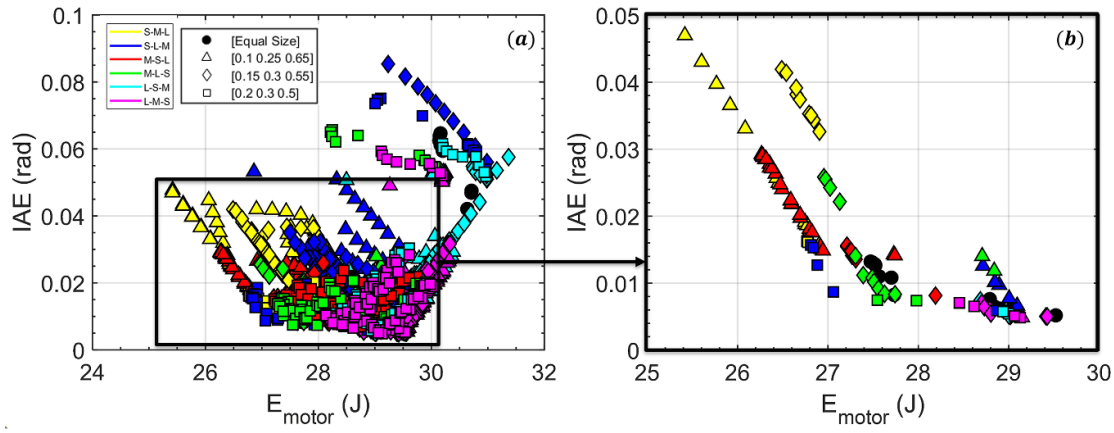

Figure 7. (a) Error vs motor energy consumption plot of each combination of MU size distribution, recruitment order, and recruitment state transition threshold tested during the simulation. (b) Plot of the Pareto frontiers for each MU size distribution. The different plot markers are used to represent the different MU size distributions, and the different plot colors are used to represent the different recruitment orders (note: S-M-L stands for Smallest-Medium-Largest, S-L-M stands for Smallest-Largest-Medium, etc). The recruitment state transition thresholds have been omitted from the plots for visual clarity.

The hydraulic oil parameters are chosen based on nominal values for ISO 32 hydraulic motor oil and the servovalve parameters are based on the datasheet for a MOOG G773 servovalve [24]. The maximum accumulator volume is chosen such that the accumulator would deplete to at least 90% of its maximum pressure over the course of a motion cycle and the maximum accumulator pressure is chosen to be a reasonable actuation pressure for hydraulic FAMs.

The P-Controller Gains for the outer control loop and the inner control loop are equal to 50 N rad^{-1} and the 0.0005 V/psi. These gains were hand-tuned based for the simulation study based on overall system performance.

4.2. Results and discussion

The IAE vs. motor energy consumption plot for each combination of MU size distribution, recruitment order, and recruitment state transition threshold is shown in figure 7, alongside a plot overlaying the Pareto frontiers for each MU size distribution (including the case for which each MU is the same size). For the other MU size distribution Pareto frontiers, there are several different recruitment orders that appear, indicating that the choice of how to recruit MUs for this test case does not always follow Henneman's size principle. In general, points with lower energy consumption and higher error are associated with recruitment orders in which the small or medium MUs are recruited first, whereas points with higher energy consumption and lower error are associated with the recruitment of the large MU first.

A global Pareto frontier, as shown in figure 8, can be constructed across the different MU size distributions to determine which size distributions within a given test case offer the best tradeoffs between performance and energetics.

Several trends can be observed from the global Pareto frontier of this test case. For one, there is not a single point with the equal MU size distribution that appears on the global Pareto frontier. This is significant because it demonstrates that for a given total bundle cross-sectional area, the tradeoff between tracking and energetic performance can be improved simply by intelligently sizing the MUs within the bundle. An additional trend that can be observed is that the points on the global Pareto frontier associated with lower energy consumption and higher error tend to have higher RS2 and RS3 recruitment state thresholds, and the points with higher energy consumption and lower error have lower RS2 and RS3 thresholds. This result is intuitive; delaying the shift to a higher RS reduces working fluid volume consumption and therefore motor energy required—but decreases control authority and force potential. However, the thresholds at which these Pareto front points occur may be unexpected. For example, one might expect that the points with the lowest energy consumption should be when both the RS2 and RS3

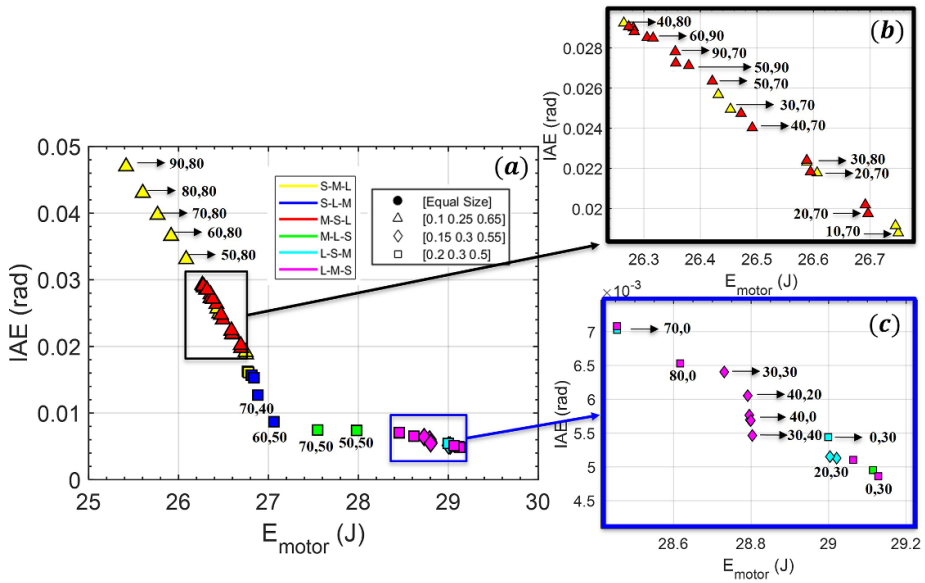

Figure 8. (a) Global Pareto frontier across MU size distributions. The ratio of maximum bundle blocked force to the maximum force required to complete the desired trajectory is equal to 2. The different plot markers are used to represent the different MU size distributions, and the different plot colors are used to represent the different recruitment orders. Selected points are also labeled with two numbers indicating the RS2 and RS3 recruitment state transition thresholds associated with that point. Due to the limited space between points, (b) and (c) provide zoomed-in callouts of the space to allow for the recruitment state thresholds to be properly labeled.

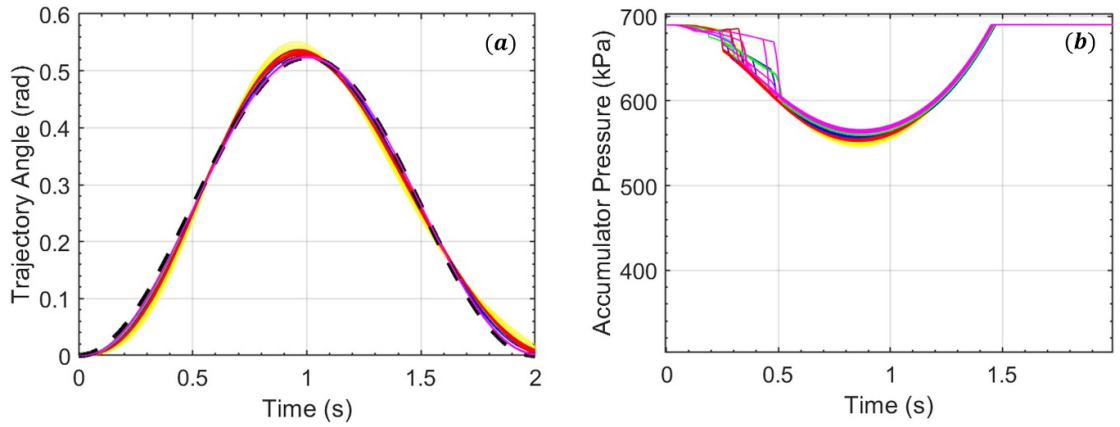

Figure 9. (a) Trajectory angle vs. time and (b) accumulator vs. time plots corresponding to the points that lie along the global Pareto frontier. Color is used to denote recruitment order, but MU size distribution is not indicated for the sake of plot visibility.

thresholds are at 90% (the largest fraction considered) of source pressure. However, this is not the case. These trends can be better understood by observing trajectory angle vs. time and accumulator pressure vs. time plots corresponding to the points on the global Pareto frontier, as shown in figure 9.

The trajectory angle vs. time plot visualizes what can be seen in the global Pareto frontier, which is that the points with lower energy consumption have higher tracking error. In the accumulator pressure plot, for the points on the Pareto frontier corresponding to the L-M-S recruitment order, it takes longer for the next MU to be recruited, and thus it takes longer for the accumulator pressure to drop. Because of the electrohydraulic coupling between the accumulator pressure and the motor driving the pump, higher accumulator pressure results in higher required motor torque, and therefore, higher required motor current. This electrohydraulic coupling largely explains why the schemes that recruit the largest MU first result in higher energy consumption, and it also explains why the recruitment state transition thresholds corresponding to the lowest energy consumption are not as straightforward as they would be for an analysis that does not consider this coupling. One final observation from the global Pareto frontier for this test case is that over half of the points on the frontier correspond to the MU size distribution that allocates 10% of overall force to the smallest MU, 15% to the medium MU, and 75% to largest MU (i.e. the most heavily biased toward the largest MU of the distributions considered). Since the range

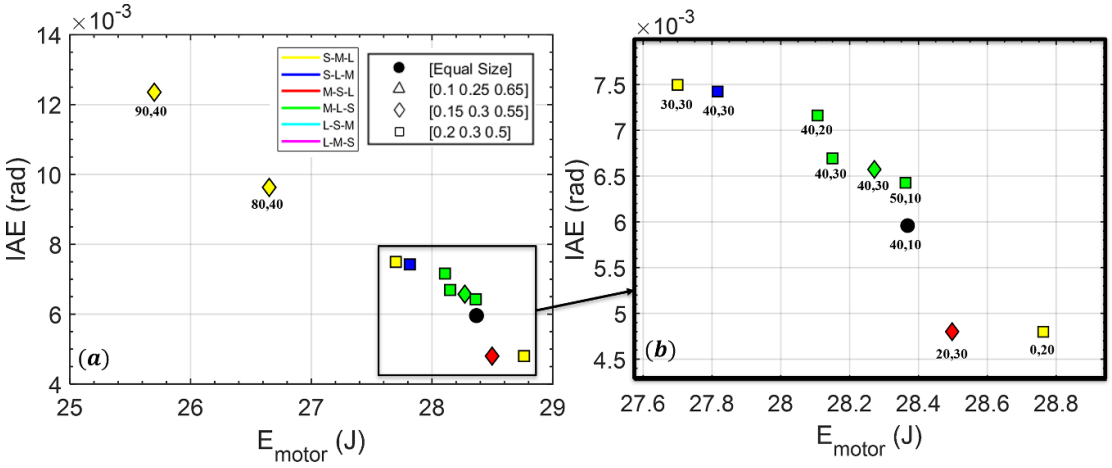

Figure 10. (a) Global Pareto frontier across MU size distributions for a bundle. The ratio of maximum bundle blocked force to the maximum force required to complete the desired trajectory is equal to 4. The different plot markers are used to represent the different MU size distributions, and the different plot colors are used to represent the different recruitment orders. Selected points are also labeled with two numbers indicating the RS2 and RS3 recruitment state transition thresholds associated with that point. Due to the limited space between points, (b) provides a zoomed-in callout of the space to allow for the recruitment state thresholds to be properly labeled.

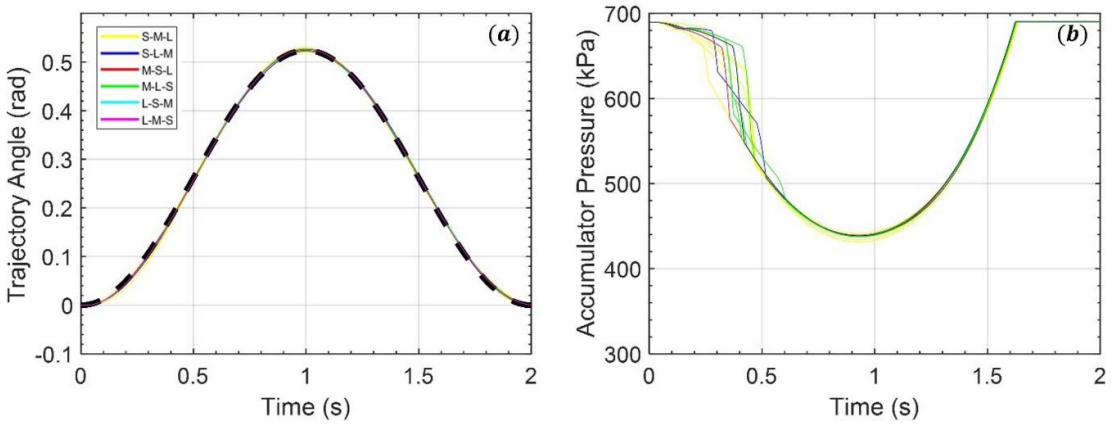

Figure 11. (a) Trajectory angle vs. time and (b) accumulator vs. time plots corresponding to the points that lie along the global Pareto frontier. Color is used to denote recruitment order, but MU size distribution is not indicated for the sake of plot visibility.

of MU size distributions tested is not exhaustive, it is not known whether this distribution is the best choice for this test case. However, there clearly exists a preferred distribution of MU sizes within a bundle that achieves the best tradeoffs between tracking performance and energetics.

To further explore how the system parameters affect the recruitment trends, an additional case study is performed. In this study, the ratio of the total bundle blocked force (which is proportional to cross-sectional area) is doubled to be equal to 4. The global Pareto frontier for this case is shown in figure 10 and the trajectory vs. time and accumulator pressure vs. time plots are shown in figure 11. The results in these plots differ significantly from those in the previous case study. For one, the global Pareto frontier does not contain a single point for which the largest MU is recruited first. In addition, both the point with the lowest energy consumption and the point with the lowest tracking error correspond to the S-M-L recruitment order.

In addition, while for the first test case the MU size distribution with the most significant size difference between the largest and smallest MU showed up most frequently, for the second test case, this size distribution did not appear at all, suggesting that there is a high degree of coupling between overall bundle force capacity and MU size distribution. The trend for the recruitment state thresholds is the same in the second test case as it is in the first test case, in which lower energy consumption/higher error is associated with higher recruitment state transition thresholds, and higher energy consumption/lower error is associated with lower recruitment state transition thresholds. The trajectory vs. time plot shows that the sensitivity of the bundle tracking to recruitment order is much lower for the second test case than it is for the first test case. This makes sense, as the bundle force capacity is

doubled, and the accumulator, while depleting more than for the first test case due to the larger size of each MU, can still provide the pressure differential required to meet the necessary flow demand to track the trajectory.

The results from both case studies show that for a given electrohydraulic system, there is a rich variable recruitment co-design problem that must consider overall bundle force capacity and MU size distribution (both of which are design parameters) in addition to the choice of recruitment order and recruitment state transition thresholds (both of which are control scheme parameters). Due to the high number of parameters and the significant coupling between the electrohydraulic system parameters and the performance metrics, the choice of MU size distribution, recruitment order, and recruitment state transition threshold is complex and motivates the application of more formal system-controller co-design optimization methods in the future.

5. Conclusions

This study examined the effects of MU size distribution, the order in which these MUs are recruited, and the pressure at which the MUs are newly recruited on variable recruitment bundle tracking and performance. To do this, two simulation-based case studies were performed for two different variable recruitment bundles with different total force capacities. The results of these case studies demonstrate that if the proper MU size distribution is chosen, recruiting new MUs from smallest to largest results in the lowest amount of energy consumption, validating the Henneman-inspired approach to variable recruitment. However, to achieve the lowest tracking error, sometimes it is desirable to recruit from largest to smallest. In addition, many of the points that lie in the middle of the global frontier, offering a compromise between tracking and energetics, correspond to the recruitment of the medium MU first, followed by either the small MU or the large MU. The results of the second case study show that if the total size of the bundle is not constrained, then a bundle size can be chosen such that it is never desirable to recruit from largest to smallest, and that either a recruitment that begins with the smallest or medium MU should always be chosen. This result is novel and shows that the optimal variable recruitment actuation strategy may not always be the Henneman-inspired approach and is constrained by the requirements of a trajectory, the maximum amount of bundle force available, and electrohydraulic system coupling.

The results of these studies also show that the choice of which recruitment state transition thresholds to use seems to be highly coupled with electrohydraulic system parameters, but as a general trend, higher recruitment thresholds coupled with the correct MU size distribution result in lower energy consumption and vice versa. The complexity of this dependence motivates the need to develop a dynamic variable recruitment scheme that can shift its transition threshold based on current loading conditions or system states, explored in close coordination with the effects of MU size distribution and recruitment order. For future work, a more exhaustive search of MU size distributions and recruitment state transition thresholds could be performed to make the results more optimal.

One of the primary limitations of this study is that it only considers a single degree-of-freedom system actuated by three motor units with a constant lever arm attachment point. Such a system was chosen for this study because it was a system that could be plausibly incorporated into hydraulically powered robots, and despite their relative simplicity, can deliver significant benefits for performance metrics like efficiency and bandwidth, as discussed earlier. The analysis performed in this study could readily be applied to multi-DOF systems, but the increased dynamic system complexity would have made it more difficult to study the relationships the electrohydraulic system parameters, actuator configuration, and recruitment control scheme. Now that some of these relationships have been established, future studies can increase the complexity of the dynamic system-of-interest. For example, a study could be performed that considers a 1-DOF system actuated by an antagonistic pair of variable recruitment FAM bundles. This would allow for the bi-directional motion typically associated with biological mammalian musculature. After this, a study with a double pendulum or triple pendulum could be performed to observe the more complicated motions typically associated with bipedal walking. However, the first thing that will be performed in future work is the experimental validation of the results for the simple system in this study.

As a final point of discussion, in this study, the fraction of desired force allocated to each MU during a trajectory was kept constant and proportional to MU size. This is the most straightforward implementation of variable recruitment, but it is not a requirement for the methods presented here. In the future, it may be useful to frame variable recruitment as a more formal dynamic control allocation problem, in which the two primary ways that force is allocated during the trajectory are through changing recruitment state transition thresholds and changing the fraction of desired force allocated to each MU. This, along with a co-design approach to finding optimal MU size distribution and electrohydraulic system parameters, will become the new dynamic variable recruitment paradigm.

Data availability statement

All data that support the findings of this study are included within the article.

Author contributions

Conceptualization, N M and M B; Funding acquisition, M B; Investigation, N M; Methodology, N M; Resources, M B; Supervision, M B; Validation, N M; Visualization, N M; Writing—original draft, N M; Writing—review and editing, M B. All authors have read and agreed to the published version of the manuscript.

Conflicts of interest

The authors declare no conflicts of interest.

Funding

This work was supported primarily by the Faculty Early Career Development Program (CAREER) of the National Science Foundation under NSF Award Number 1845203 and Program Manager Irina Dolinskaya. Additionally, this material is based upon work supported by the National Science Foundation Graduate Research Fellowship Program under Grant No. 1650114. Any opinions, findings and conclusions or recommendations expressed in this material are those of the author(s) and do not necessarily reflect those of the National Science Foundation.

ORCID iD

Nicholas Mazzoleni https://orcid.org/0000-0002-9377-849X

References

[1] Winter D A 1990 *Biomechanics and Motor Control of Human Movement* (Wiley)
[2] Mathijssen G, Schultz J A, Vanderborght B and Bicchi A 2015 A muscle-like recruitment actuator with modular redundant actuation units for soft robotics *Robot. Auton. Syst.* **74** 40–50
[3] Odhner L U and Asada H 2010 Stochastic recruitment control of large ensemble systems with limited feedback *ASME J. Dyn. Syst. Meas. Control* **132** 041008
[4] Bai X, Xue Y, Xu Y, Shang J, Luo Z and Yang J 2022 Bio-inspired new hydraulic actuator imitating the human muscles for mobile robots *Front. Bioeng. Biotechnol.* **10** 923383
[5] Bryant M, Meller M A and Garcia E 2014 Variable recruitment fluidic artificial muscles: modeling and experiments *Smart Mater. Struct.* **23** 074009
[6] Jenkins T E, Chapman E M and Bryant M 2016 Bio-inspired online variable recruitment control of fluidic artificial muscles *Smart Mater. Struct.* **25** 125016
[7] Meller M, Chipka J, Volkov A, Bryant M and Garcia E 2016 Improving actuation efficiency through variable recruitment hydraulic McKibben muscles: modeling, orderly recruitment control, and experiments *Bioinspir. Biomim.* **11** 065004
[8] Robinson R M, Kothera C S and Wereley N M 2014 Variable recruitment testing of pneumatic artificial muscles for robotic manipulators *IEEE/ASME Trans. Mechatronics* **20** 1642–52
[9] DeLaHunt S A, Pillsbury T E and Wereley N M 2016 Variable recruitment in bundles of miniature pneumatic artificial muscles *Bioinspir. Biomim.* **11** 056014
[10] Vemula D, Kim J Y, Mazzoleni N and Bryant M 2022 Design, analysis, and validation of an orderly recruitment valve for bio-inspired fluidic artificial muscles *Bioinspir. Biomim.* **17** 026001
[11] Tiwari R, Meller M A, Wajcs K B, Moses C, Reveles I and Garcia E 2012 Hydraulic artificial muscles *J. Intell. Mater. Syst. Struct.* **23** 301–12
[12] Chapman E M, Jenkins T and Bryant M 2018 Design and analysis of electrohydraulic pressure systems for variable recruitment in fluidic artificial muscles *Smart Mater. Struct.* **27** 105024
[13] Kim J Y and Bryant M 2024 Electrohydraulic system analysis of variable recruitment fluidic artificial muscle bundles with interaction effects *J. Dyn. Syst. Meas. Control* **146** 031005
[14] Henneman E, Somjen G and Carpenter D O 1965 Excitability and inhibitibility of motoneurons of different sizes *J. Neurophysiol.* **28** 599–620
[15] Hug F, Avrillon S, Ibáñez J and Farina D 2023 Common synaptic input, synergies and size principle: control of spinal motor neurons for movement generation *J. Physiol.* **601** 11–20
[16] McLean D L and Dougherty K J 2015 Peeling back the layers of locomotor control in the spinal cord *Curr. Opin. Neurobiol.* **33** 63–70
[17] Kishore S, Bagnall M W and McLean D L 2014 Systematic shifts in the balance of excitation and inhibition coordinate the activity of axial motor pools at different speeds of locomotion *J. Neurosci.* **34** 14046–54
[18] Kim J Y, Mazzoleni N and Bryant M 2021 Modeling of resistive forces and buckling behavior in variable recruitment fluidic artificial muscle bundles *Actuators* **10** 42
[19] Mazzoleni N, Kim J Y and Bryant M 2022 Motor unit buckling in variable recruitment fluidic artificial muscle bundles: implications and mitigations *Smart Mater. Struct.* **31** 035004
[20] Tondu B 2012 Modelling of the McKibben artificial muscle: a review *J. Intell. Mater. Syst. Struct.* **23** 225–53
[21] Jelali M and Kroll A 2012 *Hydraulic Servo-Systems: Modelling, Identification and Control* (Springer)
[22] Tondu B and Lopez P 2000 Modeling and control of McKibben artificial muscle robot actuators *IEEE Control Syst. Mag.* **20** 15–38
[23] Plagenhoef S, Evans F G and Abdelnour T 1983 Anatomical data for analyzing human motion *Res. Q. Exerc. Sport* **54** 169–78
[24] Moog, Inc. G773 2018 Servo valves: pilot operated flow control valve with analog interface